N O T I C E

THIS DOCUMENT HAS BEEN REPRODUCED FROM MICROFICHE. ALTHOUGH IT IS RECOGNIZED THAT CERTAIN PORTIONS ARE ILLEGIBLE, IT IS BEING RELEASED IN THE INTEREST OF MAKING AVAILABLE AS MUCH INFORMATION AS POSSIBLE

DISSOCIATIVE AND DOUBLE PHOTOIONIZATION OF CO_2 FROM THRESHOLD TO 90 Å

Toshio Masuoka* and James A. R. Samson

Behlen Laboratory of Physics
University of Nebraska-Lincoln
Lincoln, NE 68588

ABSTRACT

The molecular photoionization (CO_2^+), dissociative photoionization (CO^+, O^+ and C^+) and double photoionization (CO_2^{2+} and C^{2+}) cross sections for CO_2 have been measured from their onsets down to 90 Å by using various combinations of mass spectrometers (a coincidence time-of-flight mass spectrometer and a magnetic mass spectrometer) and light sources (synchrotron radiation, and glow and spark discharge). It is concluded that the one broad peak and the three shoulders in the total absorption cross section curve between 640 and 90 Å are caused completely by dissociative ionization processes. Several peaks observed in the cross section curve for the total fragmentation (CO^+, O^+ and C^+) are compared with those in the photoelectron spectrum reported for CO_2. The accuracy of the present cross sections is estimated to be about 10, 15 and 50% for $\sigma(CO_2^+)$, $\sigma(CO^+, O^+$ and $C^+)$ and $\sigma(CO_2^{2+}$ and $C^{2+})$, respectively.

*On leave from the Research Institute for Atomic Energy, Osaka City University, Osaka

MAR 1980
RECEIVED
NASA STI FACILITY
ACCESS DEPT.

(NASA-CR-162844) DISSOCIATIVE AND DOUBLE PHOTOIONIZATION OF CO2 FROM THRESHOLD TO 90 A (Nebraska Univ. - Lincoln.) 36 p
HC A03/MF A01 CSCL 20H

N80-19929

Unclas
G3/72 47505

I. Introduction

Since the first study of dissociative photoionization of gases at wavelengths shorter than 1000 Å some twenty years ago (1) numerous groups have reported data over the wavelength range between 304 and 1000 Å (2-7). These studies utilized mass spectrometers to identify the ionic fragments produced. With the exception of the data reported by Fryar and Browning (5) virtually all of the previously reported data suffer from underestimating the number of fragment ions produced because they are released with considerable kinetic energy relative to the parent ions. Most mass spectrometers discriminate against energetic ions. Thus, the ionic abundances quoted in the literature vary depending on the type of mass spectrometer used and on the conditions of the experiments. In fact, when the ion fragments have energies in the 5 eV range the literature values can vary by an order of magnitude or more.

It is important to know the partial cross sections for the production of the various fragment ions to improve our understanding of the molecular photoionization process. The data are also extremely valuable to our understanding of ion production in planetary and cometary atmospheres.

In the present work we report dissociative photoionization cross sections and branching ratios of ionic fragments produced from CO_2 from their thresholds down to 90 Å. The fragments observed for single ionization processes were CO_2^+, CO^+, O^+, and C^+. The doubly ionized fragments observed were CO_2^{2+} and C^{2+}. Discriminatory effects have been minimized by the use of a specially designed time-of-flight mass spectrometer.

The estimated accuracy for the branching ratios for the singly ionized fragments was ± 10 to 15% and for the doubly ionized fragments about ± 50%.

2. Experimental

A time-of-flight and a conventional magnetic sector mass spectrometer were used to study the ions produced by dissociative photoionization. The ionizing radiation sources used were (a) a dc glow discharge in helium to produce the HeI 584 Å and HeII 304 Å lines, (b) a high voltage condensed spark discharge in Ar to produce numerous discrete emission lines between 100 and 1000 Å (8), and (c) synchrotron radiation from the storage ring at the Physical Sciences Laboratory of the University of Wisconsin. The synchrotron radiation available covered the spectral range from 90 to 300 Å. In all measurements grazing incidence monochromators were used to disperse the radiation.

2.1. Time-of-flight mass spectrometer

The time-of-flight (TOF) mass spectrometer was specially constructed to minimize discriminatory effects and was operated in a coincidence mode. A schematic drawing of the coincidence TOF mass spectrometer is shown in Fig. 1. The photon beam, emerging from the exit slit of the monochromator, had a rectangular cross section of approximately 3 mm x 7 mm in the ionization chamber of the mass spectrometer. The ionization chamber consisted of two parallel plates, 25 mm apart and with circular openings (12.5 mm in diameter) covered with highly transparent wire mesh. With a voltage applied to the plates a uniform electric field, typically of the order of 1500 v/cm, was produced

perpendicular to the incoming photon beam. The positive ions and electrons produced from the photoionization of neutral molecules were accelerated in opposite directions by the high electric field. The electrons, after acceleration, were detected by an 18-stage Venetian blind electron multiplier operated in the counting mode. The electron pulses were fed through a fast preamplifier and an amplifier-discriminator and the resulting pulses used as start pulses for a time-to-amplitude converter (TAC). The ions were accelerated in the opposite direction and, after passing through a drift tube about 200 mm long which was kept at the same potential as the accelerating plate, were detected by a chevron channel electron multiplier array, the front face of which was held at a potential of -4500 V. The ion pulses after proper amplification were used as stop pulses for the TAC. The coincidence pulses obtained from the TAC were fed to a multichannel analyzer operated in the pulse height analysis mode and a mass spectrum was obtained for parent and fragmentation ions. A typical mass spectrum obtained is shown in Fig. 2 for CO_2 ionized by 304 Å radiation. Because the measurements were triggered by photoelectrons ejected from the molecules, the background or random coincidences were quite low. However, care had to be taken to collimate the photon beam to prevent it from striking any metal parts in the vicinity of the circular apertures as these photoelectrons could provide false counts.

The ratios of the fragments to the parent ions were obtained by measuring the integrated area under the various peaks corresponding to different fragments. The data acquisition time for CO_2 at 304 Å was kept at about 4800 sec. to ensure a statistical accuracy of about ± 3% for the smallest peak (CO_2^{2+}) in the mass spectrum.

The sample gas, commercially available from Matheson, was used without further purification. The sample gas pressure was typically between 5×10^{-5} and 1.5×10^{-4} torr inside the ionization region, whereas the background pressure was 7×10^{-7} torr. The background pressure increased to 1.5×10^{-6} torr when helium was introduced into the light source. No appreciable change in the fragmentation ratio could be found as a function of pressure.

2.2. Discriminatory effects of the time-of-flight mass spectrometer

Standard mass spectrometers show discrimination in the detection efficiency for various ions. Some of the discriminatory effects arising from mass and charge dependent factors in a time-of-flight mass spectrometer have been discussed previously (9, 10). The most serious discriminatory effect is that caused by the initial kinetic energy of the photodissociated fragments, causing spatial spread of the ion beam, and hence fractional losses of higher energy fragments. The kinetic energies of ion fragments formed in H_2, CO, N_2, and O_2 have been reported by Gardner and Samson (11-13). The maximum fragment energies extend from about 5 eV for N_2, O_2, and CO to 12 eV for H_2 at 304 Å. Furthermore, the angular distribution of the energetic ions can cause a non-uniform spreading of the ion beam.

The characteristics of the TOF instrument were investigated by studying the dissociative photoionization of O_2 by use of the 584 Å line. The spectrum shown in Fig. 3 is centered on mass 16 and clearly shows the situation in which the central peak arises from the O^+ thermal ions, the right hand peak from the O^+ ions with initial velocity

vectors directed away from the detector (the kinetic energy peaks at about 1 eV (13), and the left hand peak from the O^+ ions with the velocity vectors directed towards the detector. These results were obtained when the TOF mass spectrometer was operated with a low accelerating potential in the ionization chamber and with a uniform acceleration during the flight path (this was provided by 24 parallel ion-accelerating plates each with an aperture of about 12 mm in diameter). This is similar to the arrangement used by Harvey et al. (14). The lower diagram in Fig. 3 shows the effect of increasing the accelerating potential in the ion chamber only. This arrangement of the electrodes in the TOF mass spectrometer clearly illustrates that most of the ions with a lateral velocity, with respect to the instrument axis, were lost. Thus, we removed the apertures, used a high field in the ion chamber and installed a large diameter detector, as shown in Fig. 1. Assuming the drift region of the TOF instrument was field free then ions with lateral kinetic energies up to about 20 eV should still strike the detector. The actual arrangement produces acceleration and some focusing near the detector allowing ions of greater lateral energies to be collected.

Another problem that can cause discriminatory effects in a mass spectrum is that associated with the variation in secondary electron emission from the first dynode of an electron multiplier caused by ions of different masses, charges, energies, and chemical structure (15-19). If the secondary electron emission is greater than 1 electron per incident ion then there should be less discrimination between ions when the detector is used in the counting mode. No data exist for the secondary

electron emission coefficients for a CEMA. However, the various publications dealing with the detection efficiencies of channeltrons in the counting mode indicate that a plateau in the relative counting efficiency is reached for most ions with energies in excess of 4 kV (18,19). Further, the plateaus of the atomic and molecular ions studied have a maximum variation of about 10 to 20%. H_2^+ appears to deviate the most and produces the largest efficiency. Both Burrous et al. (18) and Fields et al. (19) show that their detector sensitivities are about 18% greater for H_2^+ than H^+.

Figure 4 shows the fragmentation ratio O^+/O_2^+ measured at 304 Å as a function of kinetic energy of ions impinging on the chevron CEMA. The kinetic energy of the ions was varied by changing the applied voltage (V_1) to the acceleration electrode on the electron multiplier side, while the potential (V_2) of the acceleration electrode on the ion side was kept constant. The ratio O^+/O_2^+ was found to be constant within experimental error for ions with incident energy of more than about 4.0 keV. This is a necessary although not a sufficient condition to produce a true ratio.

The ratio O^+/O_2^+ at 304 Å was measured as a function of the diameter of the ion detector by use of a variable diaphragm near the front face of the ion detector. The ratio O^+/O_2^+ increased with increasing diameter of the diaphragm but reached a saturation value as expected. The result shown in Fig. 5 clearly indicates the absence of any discriminatory effects caused by the spatial spread of the ion beams for the detector diameter larger than about 28 and 20 mm for 304 and 584 Å, respectively.

Thus, in the present design of the TOF mass spectrometer discriminatory effects have been minimized by providing an appropriate high field in

the ionization region, using a large diameter chevron CEMA (40 mm in diameter), operating in the counting mode, and by keeping the electron multiplier as close to the acceleration electrode as possible to minimize any loss of electrons caused by their initial angular distribution and energy.

2.3. Magnetic sector mass spectrometer

This instrument was a 180° magnetic sector mass analyzer based on the design of Poschenrieder and Warneck (20). Like all instruments of this type (narrow entrance and exit slits) it discriminates strongly against ions formed initially with some kinetic energy. However, because of its extremely efficient ion collection optics it could readily be used in the analog mode with conventional pico-ammeters. This allowed use of the intense spark source with its large spectral range. The spark source emits microsecond pulses and, therefore, is not readily adapted to digital counting methods, but is ideal for analog measurements.

To avoid the major problem of ion discrimination no ratios of different ions were measured. Instead, the ratio of the relative intensity of a single ion (e.g. O^+) to the intensity of the ionizing radiation was measured as a function of wavelength. With the low pressures used in the ion chamber this ratio of ions/photon is directly proportional to the photoionization cross section for this process. These relative cross sections were then placed on an absolute basis by normalizing them to the data obtained at 584 Å with the TOF mass spectrometer. The intensity of the incident radiation was measured with a calibrated electron multiplier.

This method can be expected to give good results when the kinetic energy of the ions remain constant as a function of wavelength or when the ion energies are very low as frequently encountered near the lowest threshold for dissociative photoionization. As the photon energy increases more energetic ions appear thus discrimination is likely to appear in these cross section at the higher photon energies. Examples of these effects are shown in the next section.

The data were obtained using three basic modes of operation, namely,

1. TOF mass spectrometer with dc glow discharge source (584 and 304 Å).
2. TOF mass spectrometer with synchrotron radiation source (90 - 300 Å).
3. Magnetic mass spectrometer with spark discharge source (190 - 640 Å).

In all cases the gas pressure was kept constant by use of an MKS Baratron pressure controller.

3. Results and Discussion

The analysis of the data can be performed in two separate ways in order to obtain cross section data as a function of wavelength.

Branching Ratio Method. In this case, a mass spectrum is accumulated at a given wavelength, then a branching ratio can be obtained for a specific ion by taking the ratio of the number of ions collected for that species to the total number of ions produced. When this branching ratio is multiplied by the total photoionization cross section the result is the partial photoionization cross section for producing that particular ion. This method will provide accurate partial cross sections provided there are no ions lost or discriminated against because of varying ion kinetic energies.

Ions/Photon Method. Here the wavelength is scanned for a fixed mass. The intensity of the radiation is monitored simultaneously with the ion intensity. At the low gas pressures used, the ratio of ions per incident photon is proportional to the partial photoionization cross section. As mentioned previously these relative cross sections can be put on an absolute basis by normalization at some known point.

The data obtained with the TOF mass spectrometer are assumed to be free from any serious discrimination effects. Thus, the first method, using the branching ratio measurements, was used with this instrument to determine absolute partial cross sections. The wavelength range covered was from 90 to 308 Å, using synchrotron radiation, and 584 to 304 Å radiation from a glow discharge in helium. The branching ratios are tabulated in Table 1 and the resulting partial cross sections are shown in Figs. 6-11 (data points are closed circles).

To complete the spectral coverage from the dissociative ionization threshold (642 Å) to 193 Å the spark light source was used with the magnetic mass spectrometer to measure ions/photon. Thus, relative partial cross sections were obtained. These were normalized to the TOF absolute data at 584 Å, and where necessary, for example C^+ in Fig. 9, the HeII 304 Å line was used. This method is accurate only when the kinetic energy of the ion fragment remains constant (or is small) as a function of wavelength. Provided the fragment ion is produced from a given state its kinetic energy is centered on a fixed value with a narrow energy spread given by the width of the Franck-Condon region, regardless of the energy of the photon. However, when the same fragment ion is produced from a different state its energy is usually quite different, thus, causing discriminations. The kinetic energy is usually greater for greater photon energies (11-13). This effect is illustrated in Figs. 7 and 8 for CO^+ and O^+, respectively, where the data overlap those obtained from the TOF mass spectrometer. Although the data were normalized at 584 Å to the TOF data they show severe discrimination for wavelengths shorter than 300 Å. Data obtained with this method are tabulated in Table II. However, the cross sections for a specific ion were measured independently and the sum of the branching ratios for all of the ions in Table II does not equal unity.

In the case of CO_2^+ the ions are formed with thermal kinetic energies independent of wavelength. Thus, the above problem of discrimination is absent and accurate partial cross sections for the production of CO_2^+ are obtained. As can be seen from Fig. 6 when the spark data are normalized at 584 Å to the TOF data they are also in excellent agreement

with the TOF data below 300 Å. It should be noted from Table I that 94% of the ions produced at 584 Å are CO_2^+ ions, whereas, at 304 Å only 63 % of the ions have not dissociated. The good agreement between the two sets of independent measurements implies that discrimination effects in the TOF measurements caused by the detector's unknown efficiency to ions of different mass are not serious. The scatter in the open circle data points, between 300 and 400 Å, is caused by the overlap of second order spectra that coincide with the blazed region of the diffraction grating.

The CO_2^+ cross sections decrease monotonically as a function of photon energy with no obvious structure. This is to be compared with the total photoionization cross section (21), also shown in Fig. 6, which reveals four major structures labeled A, B, C, and D (not to be confused with the spectroscopic notation). Thus, the origin of these structures must be dissociative ionization. In fact, by subtracting the partial cross section data for CO_2^+ from the total cross section we obtain the total cross section for fragmentation. These results are shown in Fig. 10.

Eland (22) has reported that the excited ion $CO_2^+(\tilde{C}\ ^2\Sigma_g^+)$ predissociates completely to fragment ions, whereas the $\tilde{X}\ ^2\Pi_g$, $\tilde{A}\ ^2\Pi_u$ and $\tilde{B}\ ^2\Pi_u^+$ states do not predissociate. Consequently the data obtained by photoelectron spectroscopy, which include the branching ratios for those states, are compared with the present results in Fig. 6, assuming that the $\tilde{X}$, $\tilde{A}$, and $\tilde{B}$ states contribute only to CO_2^+ ions. In the comparison, the same total absorption cross section shown in Fig. 6 was taken to avoid any ambiguity arising from the use of different cross

sections in the literature. There is good agreement between the present results and those reported by Brion and Tan (23), and by Samson and Gardner (24) above 500 Å. However, at shorter wavelengths the photoelectron spectroscopy data tend to be higher. This could be caused by underestimating the contribution of the $\tilde{C}$ state and other highlying dissociative states. Gustafsson et al. (25) have also reported the branching ratios for the $\tilde{X}$, $\tilde{A}$, $\tilde{B}$, and $\tilde{C}$ state of CO_2^+. Their results are in good agreement between 620 and 500 Å, whereas they are 31 and 46% high compared with the present results at 400 and 310 Å, respectively.

The only photoionization-mass spectroscopy data reported at wavelengths shorter than 600 Å are those of Weissler et al. (1) and Kronebusch and Berkowitz (4). Both sets of data show discriminatory effects caused by varying ion kinetic energies. Only the data of ref. 4 are reproduced in Fig. 6. Good agreement is found down to about 460 Å. However, as other dissociative channels open up producing ions with greater kinetic energies the branching ratios for the CO_2^+ ion become too high because of the increased loss of the more energetic ions.

The threshold for production of the fragments O^+, CO^+, and C^+ is at 19.07, 19.47 and 22.69 eV, respectively. Eland (22) has reported that at 584 Å the O^+ ion results from predissociation of the vibrationless (0,0,0) level of the $\tilde{C}\ ^2\Sigma_g^+$ state, while the CO^+ ion results from predissociation of the higher vibrational levels of the same state.

The cross sections $\sigma(CO^+)$, $\sigma(O^+)$, and $\sigma(C^+)$ are shown in Figs. 7, 8 and 9, respectively, along with those of Kronebusch and Berkowitz, in which good agreement is seen down to 400 Å for CO^+ and O^+. At shorter wavelengths, their results and our open circle data points are obviously affected by the discriminatory effect caused by the initial kinetic energies of CO^+ and O^+. For C^+, their data appear to be discriminated against at all wavelengths.

The structure in all the fragmentation curves can be correlated with the multielectron transitions observed in the photoelectron spectra reported by Brion and Tan (23), including the complete dissociation of the $\tilde{C}\ ^2\Sigma_g^+$ state. This is more obvious when their results are compared with the total fragmentation cross section in Fig. 10. These cross sections were obtained by two methods. The first method consisted simply of subtracting the CO_2^+ cross section from the total cross section (dashed line in Fig. 10). The second method was to add up the cross sections for all fragments after smoothing the data, from Table I (solid circle data points) and Table II (open circle data points). The subtraction method provides the most meaningful and accurate technique to obtain the total fragmentation cross sections over the region where discrimination occurs. However, it is interesting to note the good agreement near the dissociative-ionization threshold between the two methods. This implies that the data obtained with the magnetic mass spectrometer has little discrimination between about 475 Å and threshold. Agreement occurs as expected, with the TOF mass spectrometer data. The photoelectron data of Brion and Tan, as discussed above, show identical structure in the

fragmentation curve, leading to the conclusion that the multielectron transitions and the $\tilde{C}\ ^2\Sigma^+$ peaks, seen in the photoelectron spectra, represent dissociative ionization states. The origin of the discrepancy in the absolute amount of fragmentation in the region 200 to 500 Å between their data and the present data (dashed line) is not clear. However, the possibility of underestimating the number of continuum electrons and the contribution of the unresolved $\tilde{C}$-state must be considered. Underestimation of the number of continuum electrons is a possibility in the data of Samson and Gardner (24) shown in Fig. 10 (square box data).

The double photoionization cross sections, $\sigma(CO_2^{2+})$, and the dissociative double ionization cross sections, $\sigma(C^{2+})$, are shown in Fig. 11(a) and (b), respectively. The corresponding branching ratios are tabulated in Table I. The cross section $\sigma(C^{2+})$ is the first measurement of dissociative double ionization of CO_2 taken in the region of vacuum ultraviolet. The ratio of C^{2+} to all ions produced from CO_2 is only 0.1 - 0.4% in the region observed, which is similar to the value of 0.2% obtained with soft X-rays at 44 Å (26). The absolute magnitude of the cross sections shown in Fig. 11 is considered to be accurate only within about ± 50% because of the unknown efficiency of the detector for doubly charged ions. Recently, Tsai and Eland (27) reported the branching ratio of CO_2^{2+} at 304 Å as 0.66%, which is in good agreement with the present results of 0.7% interpolated from the data in Table I. The present data also show that the branching ratio values increase with incident photon energy and reach a plateau value of 2.6% at 200 Å. This behaviour of the branching

ratio is similar to that reported by Samson et al. (28). However, their plateau value is only about 30% of the present value. If some of the CO_2^{2+} ions have life times shorter than the flight times in the mass spectrometer, losses could be expected. In the previous experiment the flight times were of the order of 5 to 10 μs, whereas, in the present measurements the flight time was about 2 μs (see Fig. 2). There have been two values reported in the literature for the lifetime of CO_2^{2+}, namely, 2.3 μs and 21.6 μs by electron impact (29) and photon impact (27) methods, respectively. Thus, the present results could be expected to observe more doubly charged ions than observed by ref. 28.

It is also possible that some CO_2^{2+} ions have extremely short life times and essentially dissociate immediately producing the following fragments,

$$CO_2^{2+} \longrightarrow CO^+ + O^+$$
$$C^+ + O^+ + O$$
$$O^+ + O^+ + C$$

The minimum thresholds for each of these processes are 33.1, 41.5, and 43.8 eV, respectively. Each of the fragments CO^+, C^+, and O^+ shown in Figs. 7-9 show structure in these cross sections between 40 and 60 eV.

Lee et al. (30) have observed undispersed vacuum ultraviolet fluorescence from CO_2 excited by synchrotron radiation in the wavelength region 175 - 800 Å. In particular, they observe a broad band of fluorescence between 175 and 530 Å that bears a striking resemblance to the shape of the total fragmentation curve (Fig. 10). The absolute fluorescence cross sections are about 5 - 10% of the total fragmentation

cross section. It appears certain that the fluorescence originates from excited fragments produced by dissociative photoionization.

ACKNOWLEDGEMENT

This research was supported by the Planetary Atmospheres Program of the National Aeronautics and Space Administration under Grant No. NGR 28-004-021.

We wish to thank Dr. P. R. Woodruff in Physical Sciences Laboratory for her help in setting up the experimental system at the synchrotron site. We also wish to express our appreciation to Drs. S. Leach and P. Guyon of the University of Paris-Sud for their helpful discussions in the early design of the TOF mass spectrometer.

TABLE I. Branching ratios for dissociative and double photoionization of CO_2 obtained by TOF mass spectrometer.

Wavelength (Å)	CO_2^+	CO^+	O^+	C^+	CO_2^{2+}	C^{2+}
89.6	0.28	0.12	0.37	0.21	0.027	0.0036
99.5	0.29	0.12	0.36	0.21	0.026	0.0024
109.4	0.30	0.12	0.35	0.20	0.027	0.0024
119.3	0.32	0.12	0.35	0.18	0.027	0.0018
129.2	0.34	0.13	0.34	0.18	0.026	0.0018
139.2	0.36	0.12	0.32	0.17	0.028	0.0010
149.2	0.37	0.13	0.31	0.16	0.025	0.0012
159.0	0.39	0.13	0.30	0.16	0.026	0.0011
168.9	0.41	0.13	0.28	0.15	0.026	
178.8	0.43	0.14	0.27	0.14	0.025	
188.7	0.44	0.14	0.27	0.14	0.027	
198.6	0.44	0.14	0.26	0.14	0.026	
208.5	0.44	0.14	0.26	0.14	0.025	
218.4	0.45	0.14	0.25	0.13	0.024	
228.4	0.48	0.14	0.24	0.12	0.023	
238.3	0.51	0.14	0.22	0.11	0.019	
248.2	0.55	0.13	0.20	0.10	0.018	
258.0	0.60	0.12	0.18	0.091	0.016	
268.0	0.63	0.11	0.17	0.082	0.013	
277.9	0.64	0.11	0.16	0.078	0.012	
287.8	0.64	0.11	0.16	0.081	0.010	
297.7	0.63	0.11	0.17	0.086	0.0091	
304[a]	0.63	0.096	0.17	0.10	0.012	
307.6	0.62	0.11	0.18	0.092	0.0060	
584[a]	0.94	0.019	0.045			

[a]Measured with a glow discharge

TABLE II. Branching ratios for dissociative photoionization of CO_2 obtained by magnetic mass spectrometer.

Wavelength (Å)	CO_2^+	CO^+	O^+	C^+
192.6	0.49	0.075	0.091	0.12
215.2	.53	.082	.080	.11
220.7	.51	.087	.079	.12
230.9	.46	.075	.073	.11
250.9	.57	.078	.083	.11
257.0	.56	.074	.073	.092
260.3	.53	.063	.065	.081
279.9	.61	.080	.085	.080
282.4	.63	.075	.087	.085
292.6	.52	.061	.085	.081
294.3	.54	.069	.090	.073
297.7	.56	.074	.10	.085
304[a]	.59			
307.5	.49	.077	.11	.094
329.0	.43	.088	.12	.10
337.3	.57	.086	.12	.10
351.4	.67	.095	.12	.094
363.0	.68	.096	.13	.082
374.7	.58	.086	.10	.056
390.0	.62	.080	.11	.035
405.4	.66	.088	.10	.021
410.0	.69	.098	.11	.017
415.9	.74	.11	.11	.014
436.7	.66	.094	.088	
442.2	.74	.11	.097	
447.0	.76	.11	.092	
449.7	.81	.10	.089	
457.5	.80	.096	.086	
459.3	.83	.097	.090	
462.0	.77	.086	.084	

TABLE II (cont.)

Wavelength (Å)	CO_2^+	CO^+	O^+
465.4	.81	.092	.085
471.5	.86	.088	.085
475.3	.76	.071	.074
479.4	.77	.069	.073
486.6	.87	.071	.075
491.7	.87	.059	.074
495.9	.92	.057	.071
500.2	.83	.047	.067
508.5	.88	.040	.067
514.0	.88	.047	.065
519.4	.89	.034	.065
522[a]	.92		
526.5	.96	.031	.061
537[a]	.89		
538.5	.99	.028	.059
544.7	.87	.025	.055
548.9	.90	.024	.049
551.4	.92	.025	.048
555.5	.93	.024	.053
558.5	.99	.030	.050
564.4	.94	.035	.051
571.0	.96	.029	.042
584[a]	.94		
585.8	.95	.015	.041
594.1	.93	.018	.043
596.7	.88	.011	.041
609.9	.97	.003	.042
619.1	.97	.014	.038
630.3	.94	.004	.033
634.3	1.02	.003	.035
637.3	.98		.033
641.5	.95		.007

[a]Measured with a glow discharge

REFERENCES

1. G. L. Weissler, J. A. R. Samson, M. Ogawa, and G. R. Cook. - J. Opt. Soc. Am., 1959, 49, 338-349.

2. V. H. Dibeler and J. A. Walker. - J. Opt. Soc. Am., 1967 57, 1007-1012.

3. K. E. McCulloh. - J. Chem. Phys., 1973, 59, 4250-4259.

4. P. L. Kronebusch and J. Berkowitz. - Int. J. Mass Spectrom. Ion Phys., 1976, 22, 283-306.

5. J. Fryar and R. Browning. - Planet. Space Sci., 1973, 21, 709-711.

6. R. Browning, J. Fryar, and R. Cunningham. - Advan. Mass Spectrom., 1974, 6, 933-937.

7. B. Brehm. - Z. Naturforschg, 1966, 21a, 196-209.

8. J. A. R. Samson. - *Techniques of Vacuum Ultraviolet Spectroscopy* (Wiley & Sons, New York 1967).

9. R. J. Van Brunt, G. S. Lightner, and W. D. Whitehead. - Rev. Sci. Instrum., 1971, 42, 1052-1059.

10. W. W. Hunt, K. E. McGee, J. K. Streeter, and S. E. Maughan. - Rev. Sci. Instrum., 1968, 39, 1793-1799.

11. J. L. Gardner and J. A. R. Samson. - Phys. Rev., 1975, A12, 1404-1407.

12. J. L. Gardner and J. A. R. Samson. - J. Chem. Phys., 1975, 62, 1447-1452.

13. J. L. Gardner and J. A. R. Samson. - J. Chem. Phys., 1975, 62, 4460-4463.

14. A. Harvey, M. F. Monteiro, and R. I. Reed. - Int. J. Mass Spectrom. Ion Phys., 1970, 4, 365-377.

15. B. L. Schram, A. J. H. Boerboom, W. Kleine, and J. Kistemaker. - Physica, 1966, 32, 749-761.

16. M. Van Gorkom and R. E. Glick. - Int. J. Mass Spectrosc. and Ion Phys., 1970, 4, 203-218.

17. M. G. Inghram and R. J. Hayden. - *Mass Spectroscopy*, Nuclear Science Series, Report 14, NAS-NRC, Washington, 1954, p. 44.

18. C. N. Burrous, A. J. Lieber, and V. T. Zaviantseff. - Rev. Sci. Instrum., 1967, 38, 1477-1481.

19. S. A. Fields, J. L. Burch, and W. A. Oran. - Rev. Sci. Instrum., 1977, 48, 1076-1078.

20. W. Poschenrieder and P. Warneck. - J. Appl. Phys., 1966, 37, 2812-2820.

21. J. A. R. Samson and G. N. Haddad, unpublished.

22. J. H. D. Eland. - Int. J. Mass Spectrom. Ion Phys., 1972, 9, 397-406.

23. C. E. Brion and K. H. Tan. - Chem. Phys., 1978, 34, 141-151.

24. J. A. R. Samson and J. L. Gardner - unpublished.

25. T. Gustafsson, E. W. Plummer, D. E. Eastman and W. Gudat. - Phys. Rev., 1978, A17, 175-181.

26. R. J. Van Brunt, F. W. Powell, R. G. Hirsch and W. D. Whitehead. - J. Chem. Phys., 1972, 57, 3120-3129.

27. B. P. Tsai and J. H. D. Eland, - to be published in Int. J. Mass Spectrom. Ion Phys., 1980.

28. J. A. R. Samson, P. C. Kemeny and G. N. Haddad. - Chem. Phys. Letters, 1977, 51, 75-76.

29. A. S. Newton and A. F. Sciamanna. - J. Chem. Phys., 1964, 40, 718-723.

30. L. C. Lee, R. W. Carlson, D. L. Judge and M. Ogawa. - J. Chem. Phys., 1975, 63, 3987-3995.

31. F. H. Dorman and J. D. Morrison. - J. Chem. Phys., 1961, 35, 575.

FIGURE CAPTIONS

Fig. 1. A schematic diagram of the coincidence time-of-flight mass spectrometer. The width of the light beam was about 3 mm. The separation of the ion plates was 25 mm and the ion and electron extraction holes had a diameter of 12.5 mm.
A: experimental condition used with a glow discharge.
B: experimental condition used with synchrotron radiation.

Fig. 2. A typical time-of-flight mass spectrum obtained for CO_2 at 304 Å in which all possible fragments except O_2^+ are observed, including CO_2^{2+}.

Fig. 3. Time-of-flight mass spectra of O_2 obtained at 584 Å, which show the kinetic energy distribution of O^+. a) the field strength in the ionization chamber was 11.8 V/cm.
b) the field strength was 52.8 V/cm. These spectra were obtained with a narrow flight tube that discriminated against energetic ions. A time scale is shown in the figure to identify the width of arrival time. The central peak is arbitrarily centered on 0.5 μs.

Fig. 4. The fragmentation ratio O^+/O_2^+ measured at 304 Å as a function of kinetic energy of ions impinging on the chevron CEMA. The ratio O^+/O_2^+ is proportional to $\eta(O^+)P(O^+)/\eta(O_2^+)P(O_2^+)$, where $\eta(O^+)$ and $\eta(O_2^+)$ are the detection efficiencies of the chevron CEMA for O^+ and O_2^+, respectively, and $P(O^+)$ and $P(O_2^+)$ are the loss probabilities of O^+ and O_2^+, respectively, in the drift tube. As $P(O^+)/P(O_2^+)$ is constant over a certain range of the dectector diameter as shown in Fig. 5, it is obvious that $\eta(O^+)/\eta(O_2^+)$ is also constant.

Fig. 5. Variations of the fragmentation ratio O^+/O_2^+ at 584 and 304 Å as a function of the ion detector diameter.

Fig. 6. Partial photoionization cross sections for CO_2^+ as a function of wavelength. ●, present results from Table I; o, present results from Table II; ▲, Kronebusch and Berkowitz (ref. 4); □, Samson and Gardner (ref. 24); ☆, Brion and Tan (ref. 23); •, total absorption cross sections (ref. 21). The bars show the reproducibility of the results obtained from three experimental runs.

Fig. 7. Partial dissociative photoionization cross sections for CO^+ as a function of wavelength. O, present results from Table II; ●, present results from Table I; ▲, Kronebusch and Berkowitz (ref. 4). The vertical arrow indicates the thermochemical onset for CO^+.

Fig. 8. Partial dissociative photoionization cross sections for O^+ as a function of wavelength. O, present results from Table II; ●, present results from Table I; ▲, Kronebusch and Berkowitz (ref. 4). The vertical arrow indicates the thermochemical onset for O^+.

Fig. 9. Partial dissociative photoionization cross sections for C^+ as a function of wavelength. O, present results from Table II; ●, present results from Table I; ▲, Kronebusch and Berkowitz (ref. 4). The vertical arrow indicates the thermochemical onset for the process $C^+ + 2O$, while the onset for $C^+ + O_2$ is at 544 Å. The latter is not likely for the symmetric triatomic molecule.

Fig. 10. Cross sections for the total fragmentation as a function of wavelength. O, present results from Table II, (see the text); ●, present results from Table I; ——·——, present results (subtraction method, see the text); ▲, Kronebusch and Berkowitz (ref. 4); ☆, Brion and Tan (ref. 23).

Fig. 11. a. Double photoionization cross sections for CO_2^{2+} and b. dissociative double ionization cross sections for C^{2+} as a function of wavelength. ●, present results from Table I. The error bars show the counting statistics. The vertical arrow indicates the onset for CO_2^{2+} reported by Dorman and Morrison (ref. 31) and the thermochemical onset for C^{2+}.

ORIGINAL PAGE IS
OF POOR QUALITY

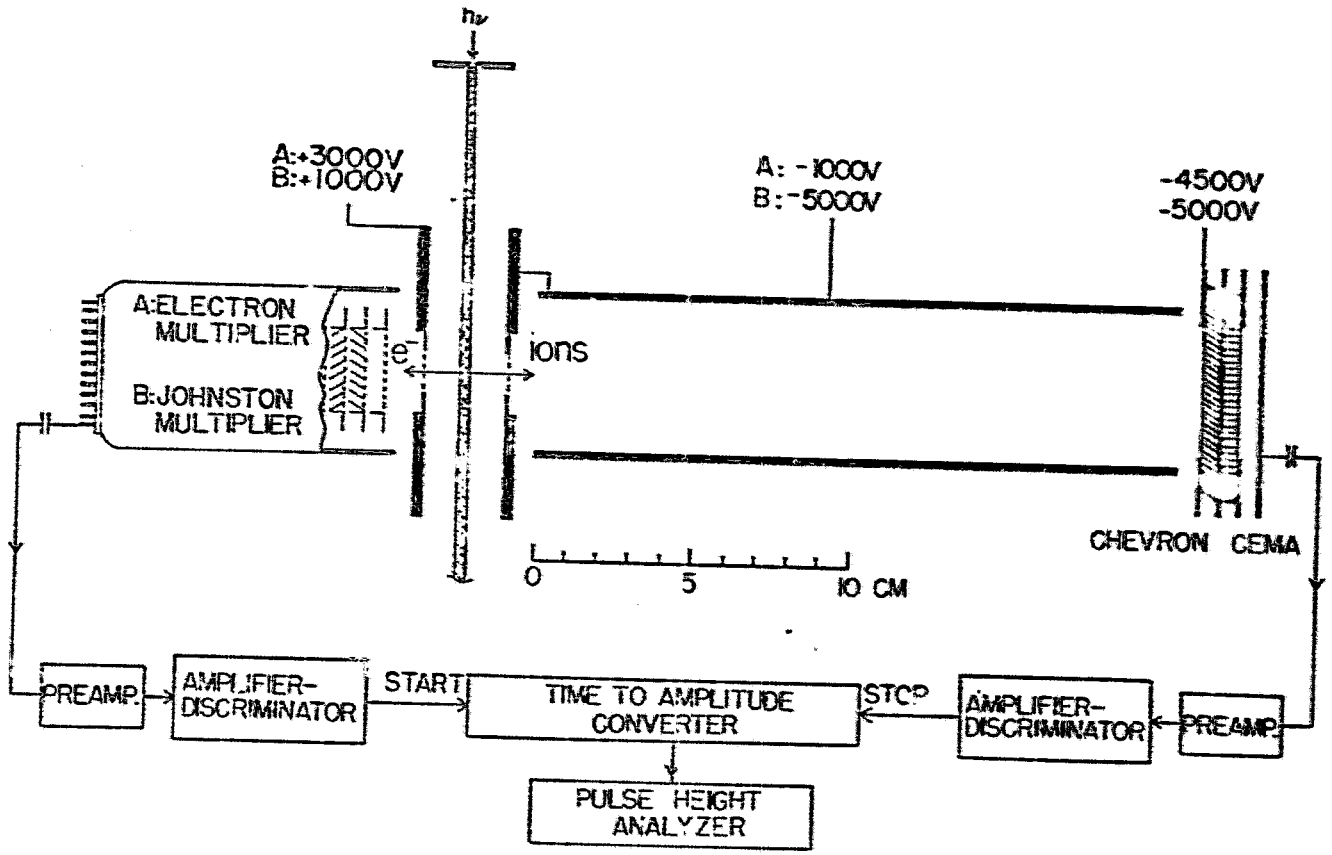

Masuoka and Samson Fig. 1

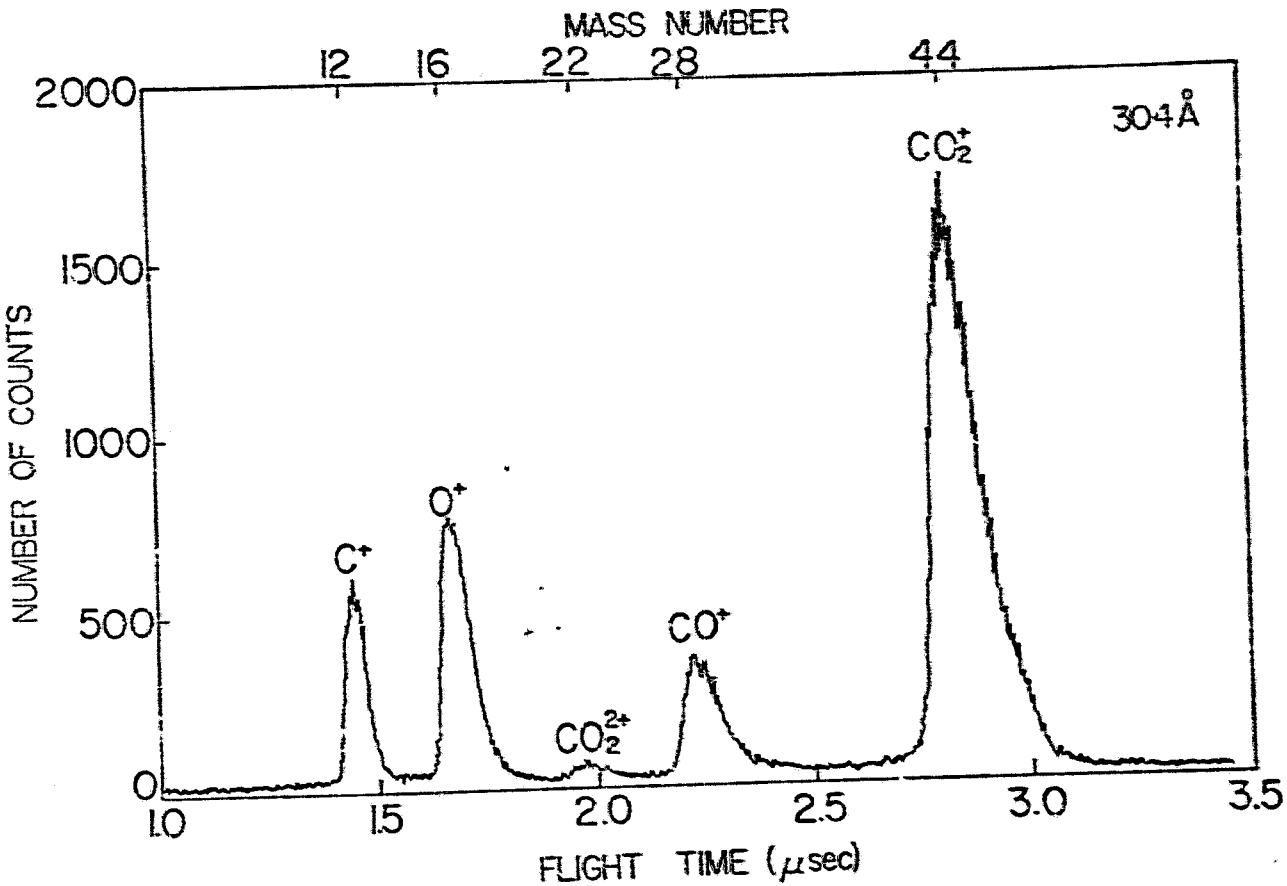

Masuoka and Samson Fig. 2

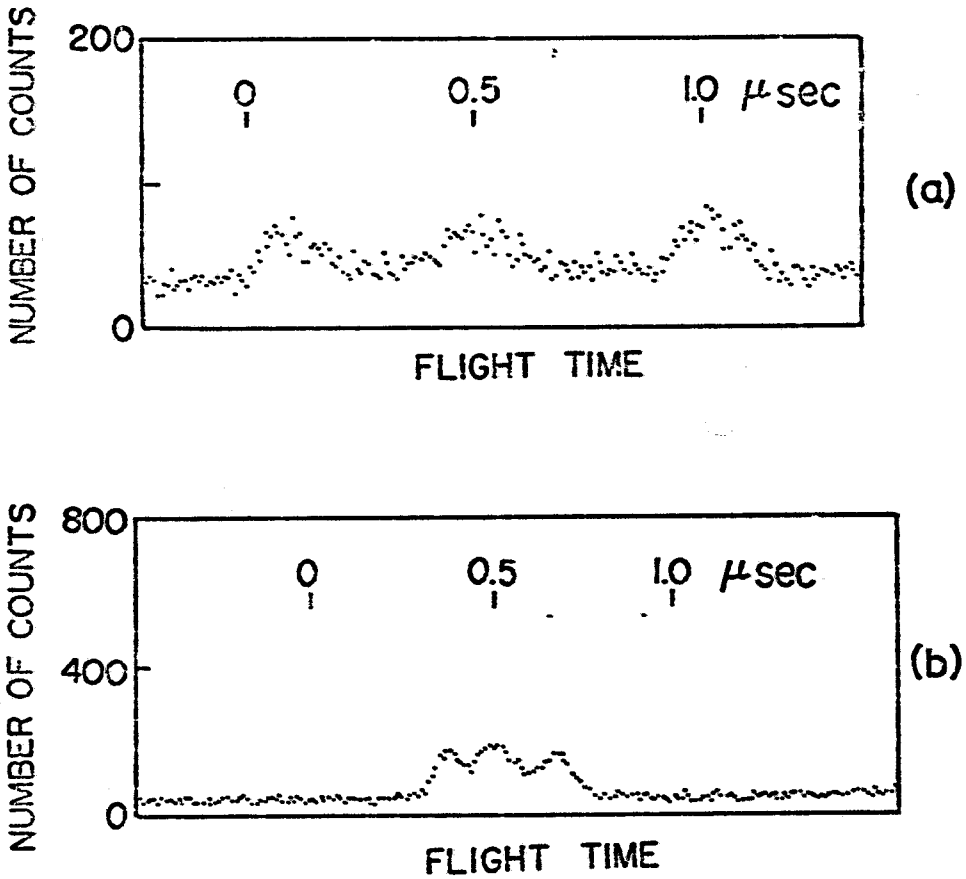

Masuoka and Samson Fig. 3

ORIGINAL PAGE IS
OF POOR QUALITY

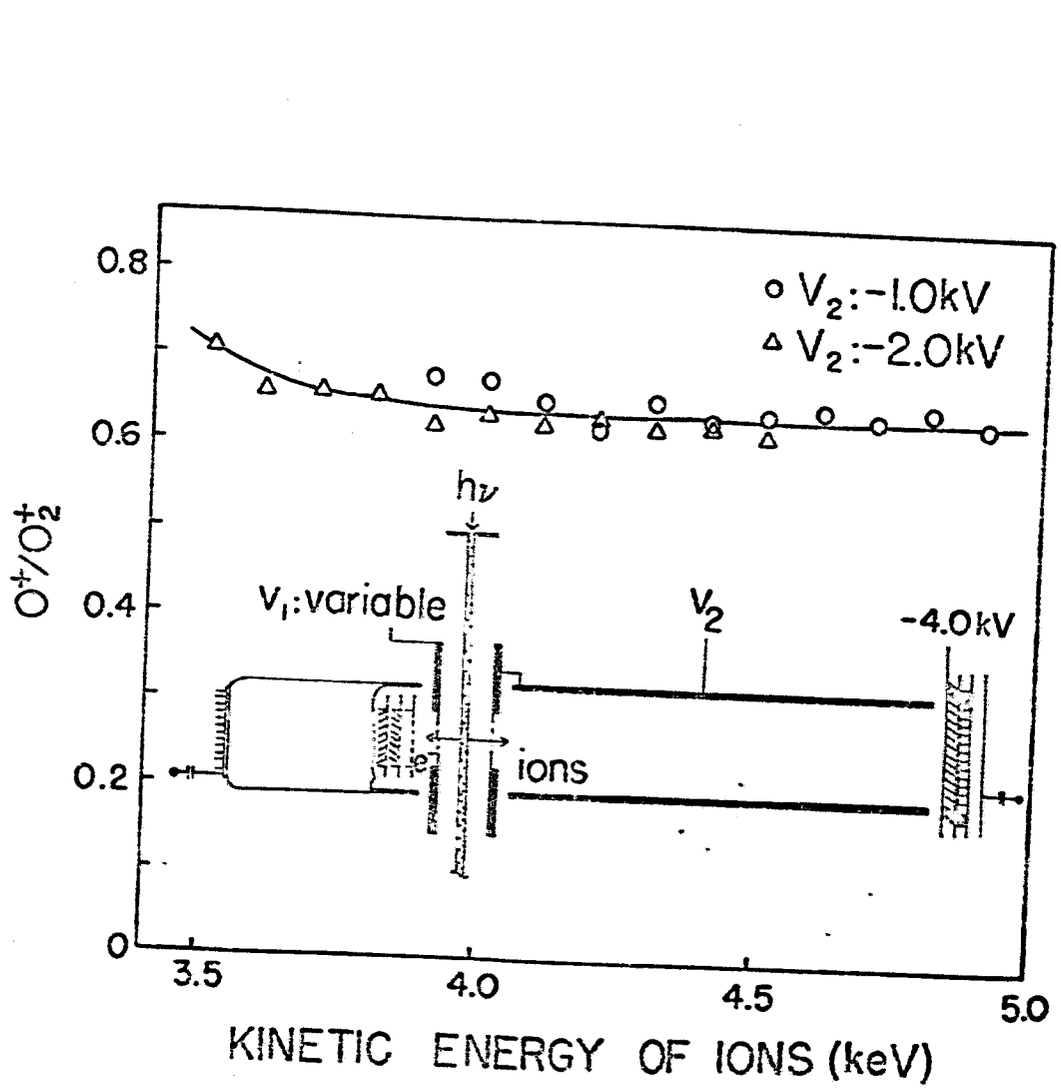

Masuoka and Samson Fig. 4

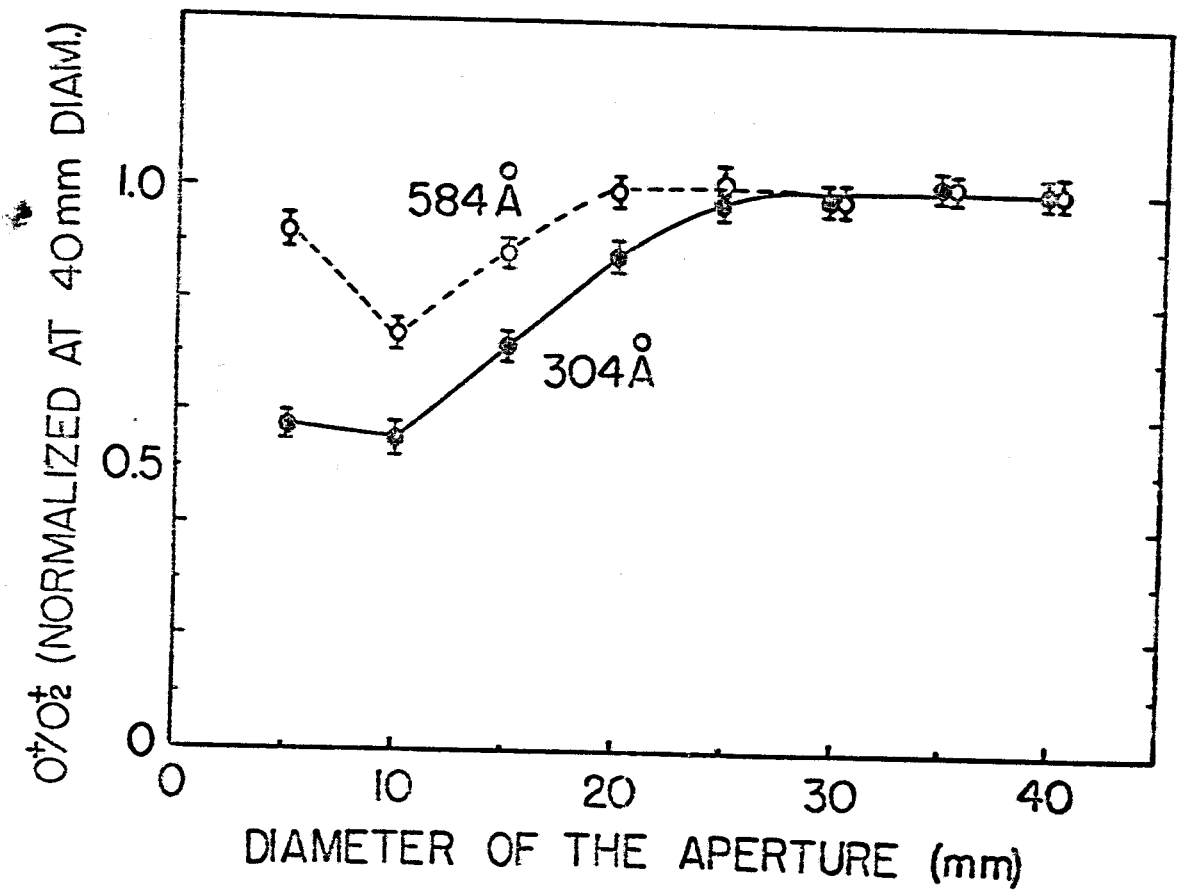

Masuoka and Samson Fig. 5

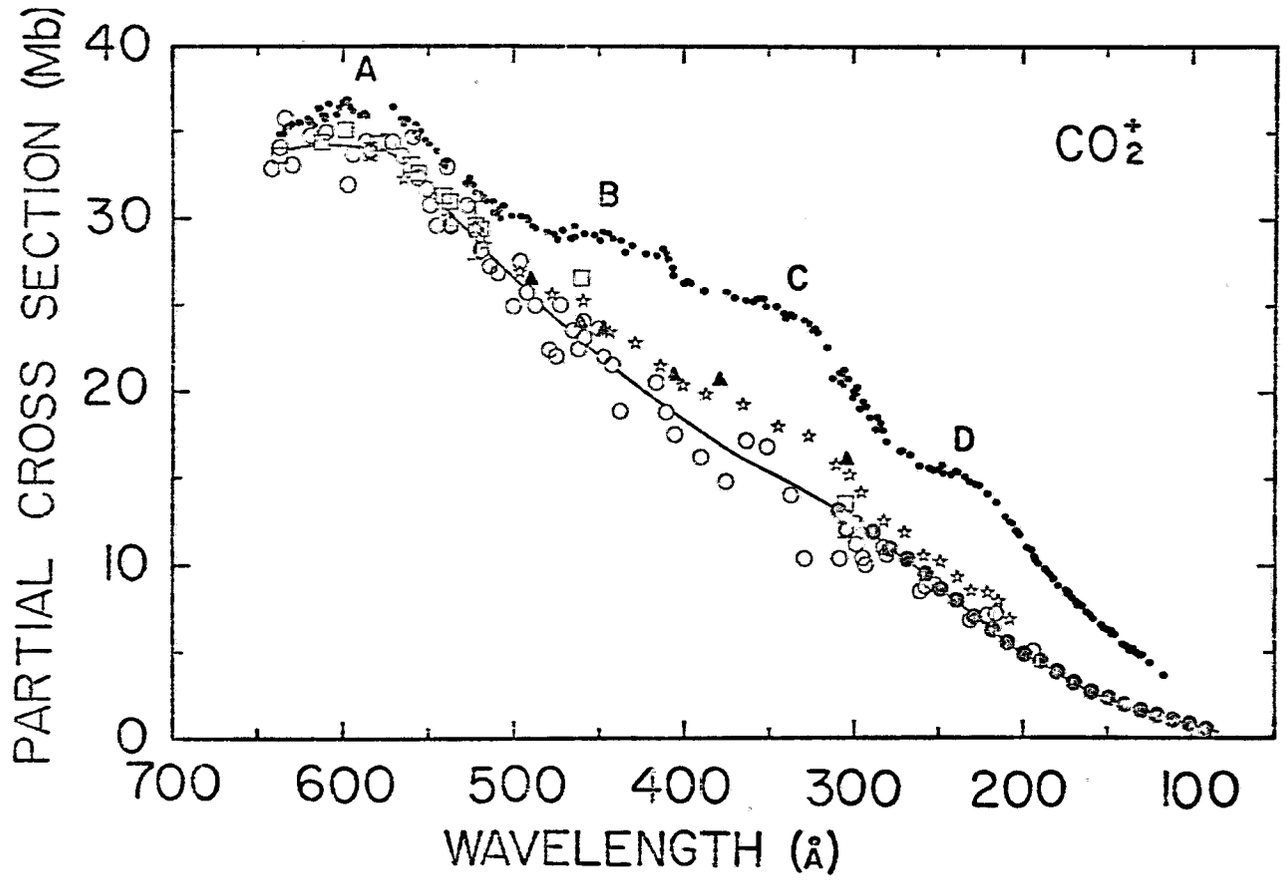

Masuoka and Samson Fig. 6

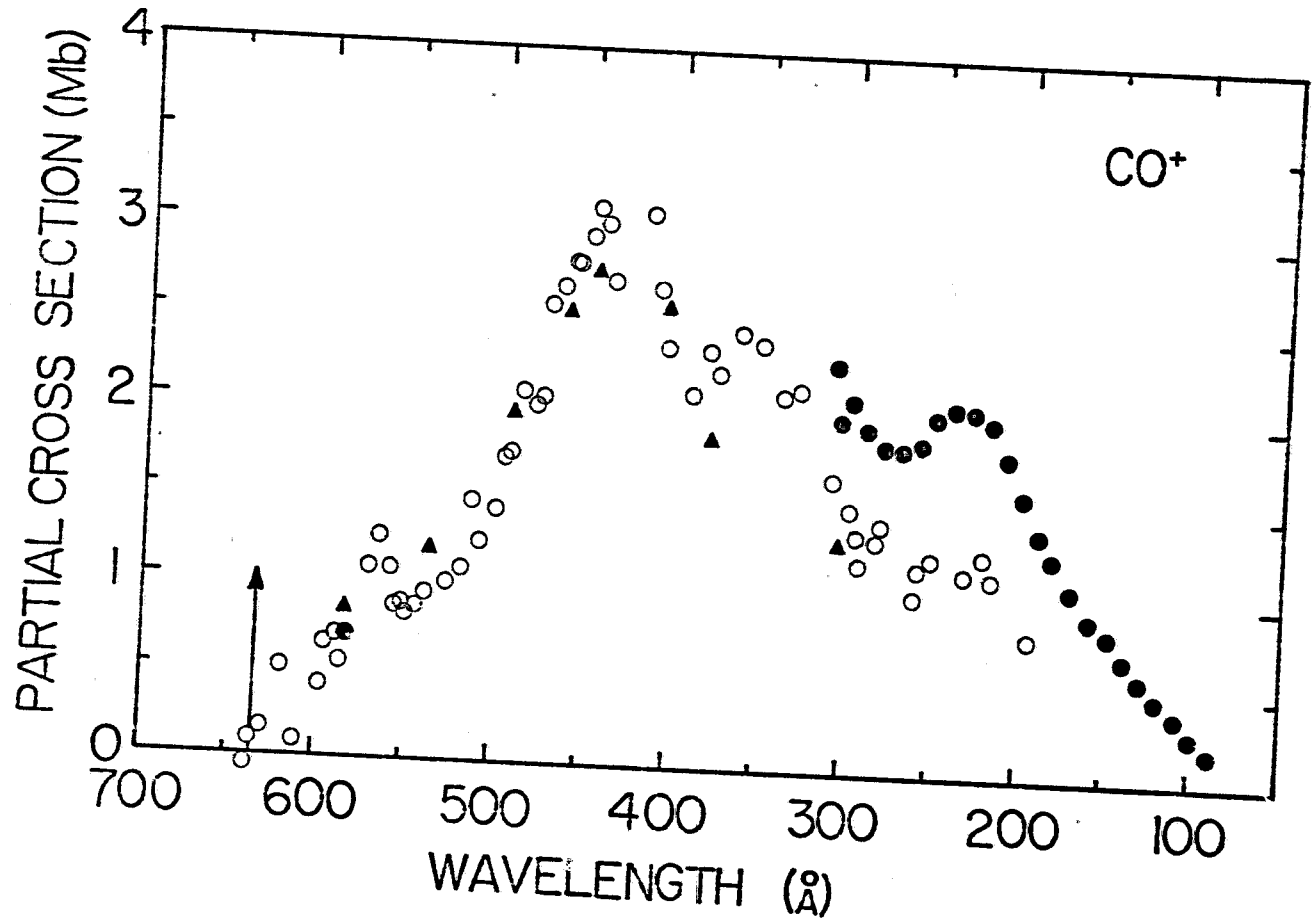

PARTIAL CROSS SECTION (Mb)
4
3
2
1
0
700
600
500
400
300
200
100
WAVELENGTH (Å)
CO+

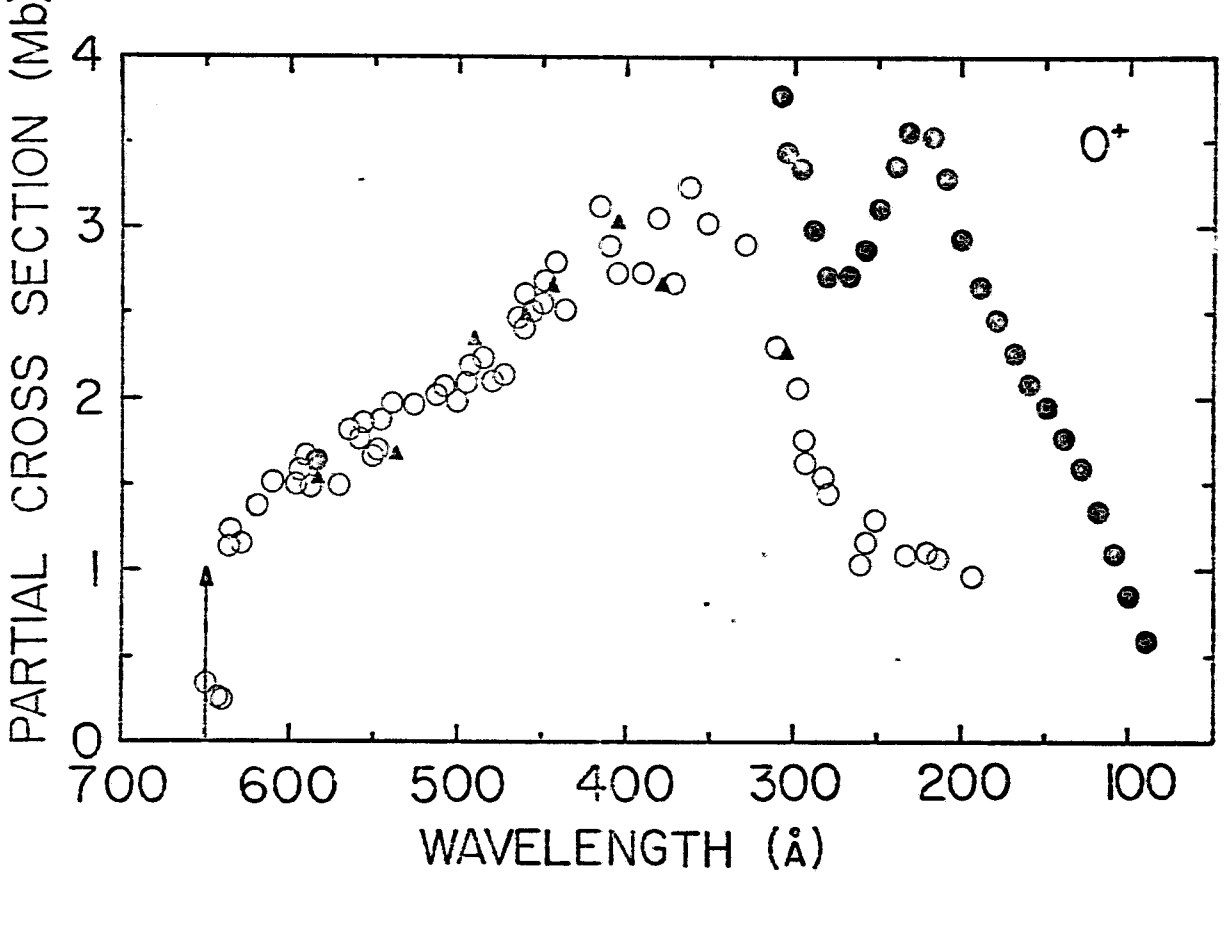

Masuoka and Samson Fig. 8

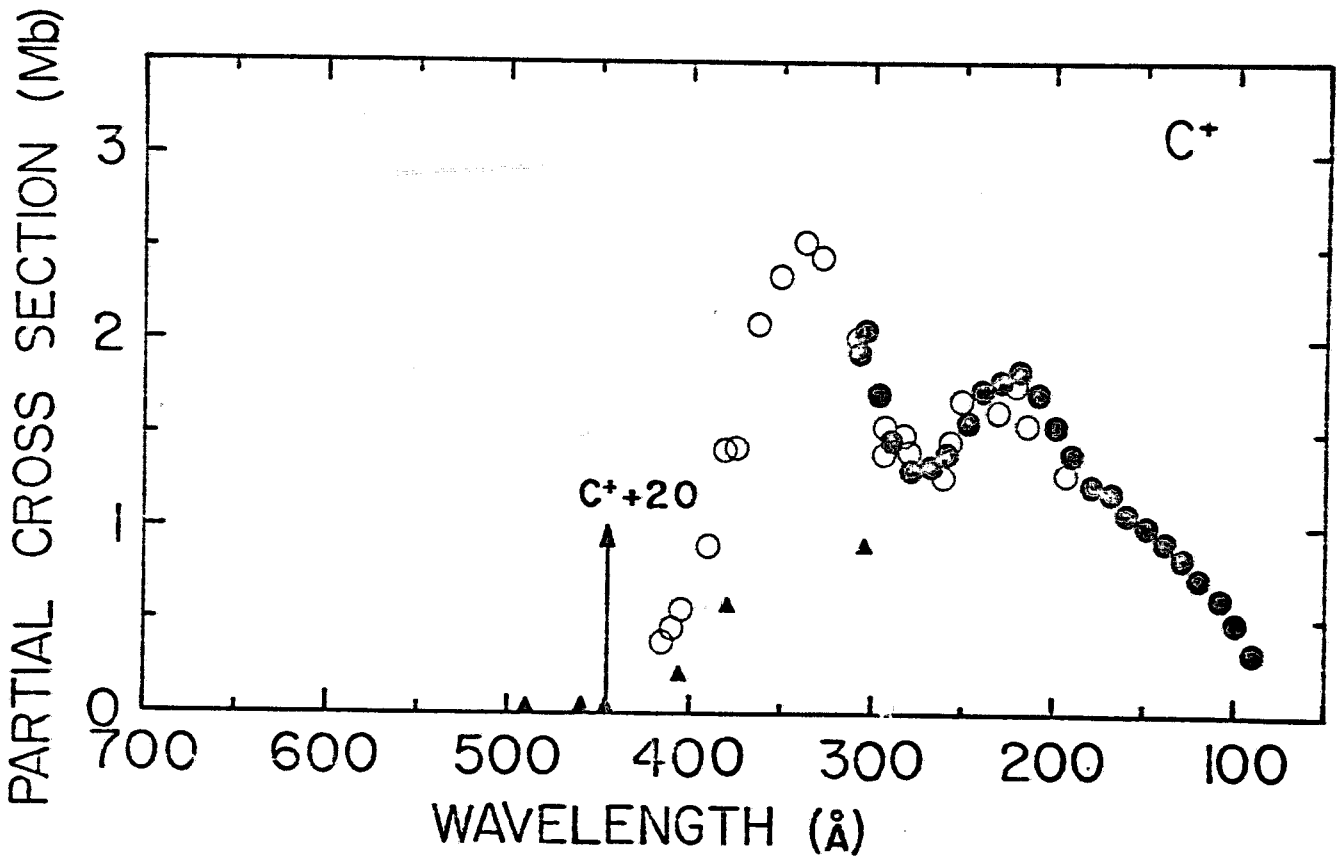

Masuoka and Samson Fig. 9

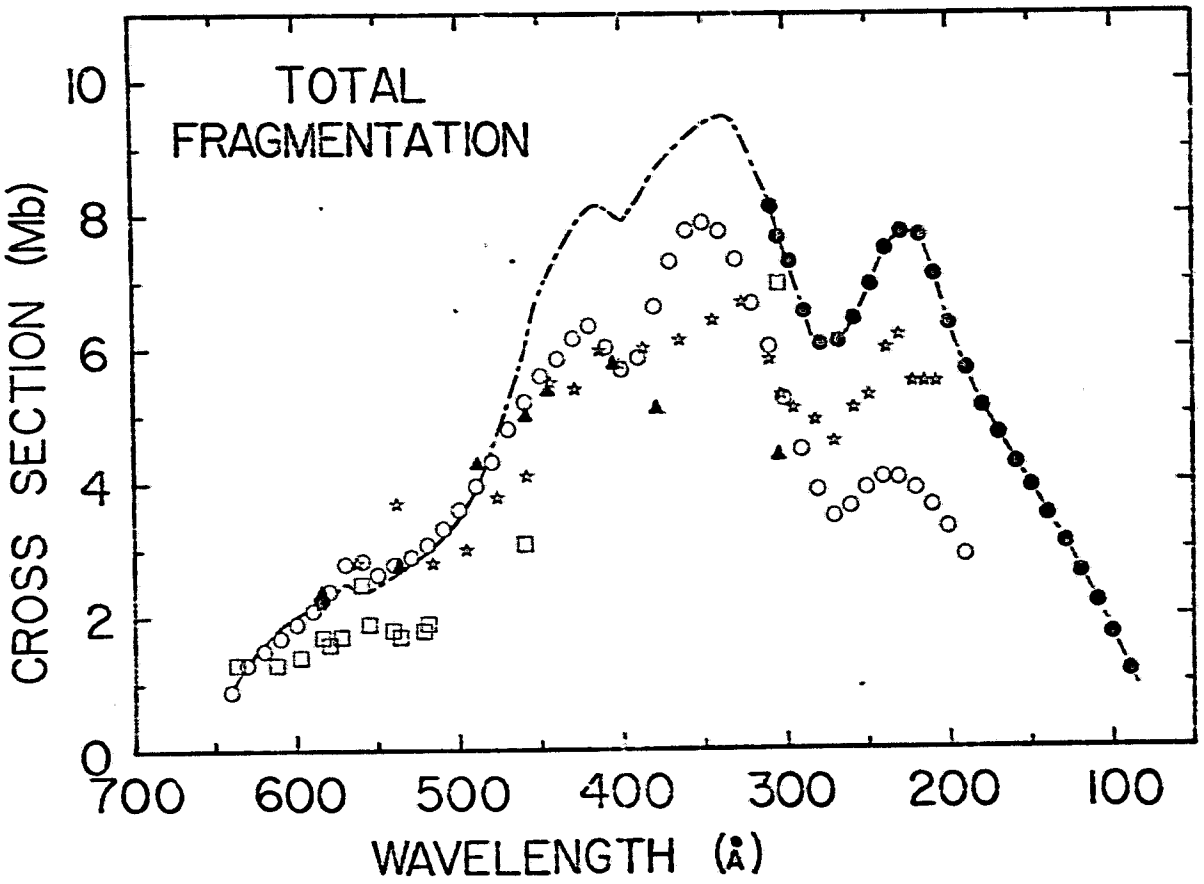
TOTAL
FRAGMENTATION
CROSS SECTION (Mb)
0
2
4
6
8
10
700
600
500
400
300
200
100
WAVELENGTH (Å)

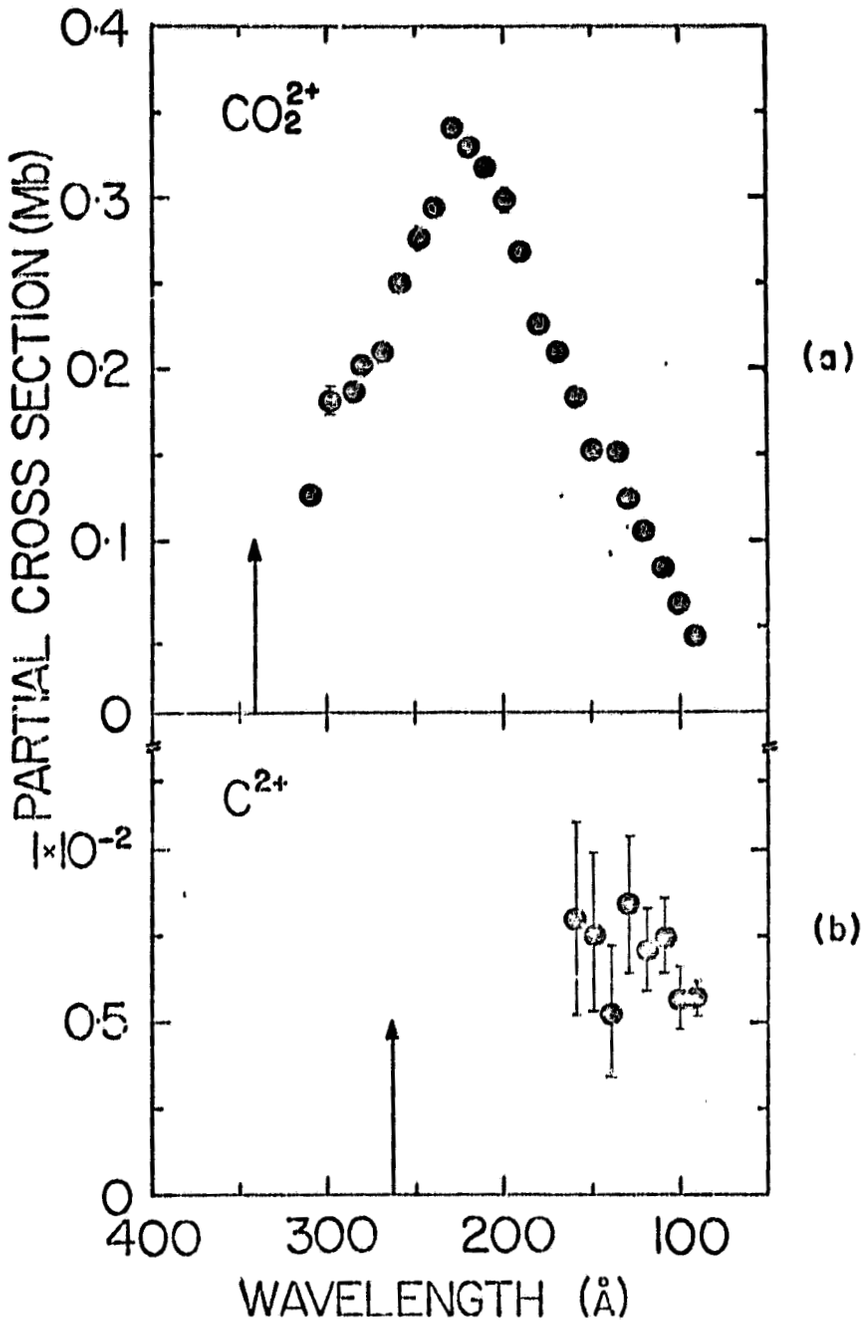

Masuoka and Samson Fig. 11